Geochemical Perspectives Letters

Thermodynamic controls on redox-driven kinetic stable isotope fractionation

C. Joe-Wong[1]*, K.L. Weaver[2], S.T. Brown[3], K. Maher[2]

OPEN ACCESS

doi: 10.7185/geochemlet.1909

Abstract

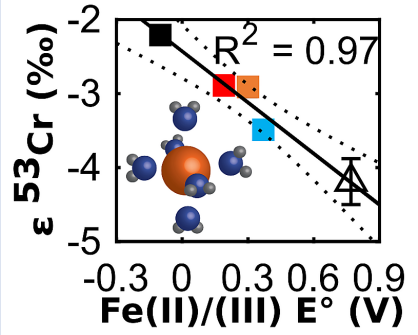

Stable isotope fractionation arising from redox reactions has the potential to illuminate the oxygenation of Earth's interior, oceans, and atmosphere. However, reconstruction of past and present redox conditions from stable isotope signatures is complicated by variable fractionations associated with different reduction pathways. Here we demonstrate a linear relationship between redox-driven kinetic fractionation and the standard free energy of reaction for aqueous chromium(VI) reduction by iron(II) species. We also show that the intrinsic kinetic fractionation factor is log-linearly correlated with the rate constant of reaction, which is in turn a function of the free energy of reaction. The linear free energy relationship for kinetic fractionation describes both our experimental results and previous observations of chromium isotope fractionation and allows the magnitude of fractionation to be directly linked to environmental conditions such as pH and oxygen levels. By demonstrating that the magnitude of kinetic fractionation can be thermodynamically controlled, this study systematically explains the large variability in chromium(VI) isotope fractionation and provides a conceptual framework that is likely applicable to other isotope systems.

Received 30 October 2018 | Accepted 26 February 2019 | Published 29 March 2019

Introduction

Stable isotope fractionation is used to examine Earth processes ranging from the evolution of redox conditions in ancient oceans (Frei *et al.*, 2009) to the fate of modern contaminant plumes (Ellis *et al.*, 2002). Interpreting the isotopic signatures observed in these systems requires frameworks to link fractionation to environmental variables. For instance, fractionation during precipitation can be modelled as a function of solvation energies and the composition of ions in solution or the balance between forward and backward reaction rates (Fantle and DePaolo, 2007; DePaolo, 2011; Hofmann *et al.*, 2012; Nielsen *et al.*, 2012). Similarly, Kavner and colleagues have shown that kinetic fractionation during metal electroplating scales linearly with the standard electrode potential ($E°$) (Kavner *et al.*, 2005, 2008). However, if the standard electrode potential is taken to be analogous to the free energy of reaction ($\Delta G_r°$) in natural soils and sediments, this relationship has not yet been demonstrated for non-electrochemical reactions.

Knowledge of the thermodynamic controls on kinetic fractionation could be used to interpret redox-driven isotope fractionation in natural systems. The relationship between thermodynamic parameters ($E°$ or $\Delta G_r°$) and the kinetics of electron transfer can be formalised *via* Marcus theory (Marcus, 1964, 1965, 1993). Unlike other models that link changes in observed fractionation with shifts between kinetic and equilibrium fractionation (DePaolo, 2011), Marcus theory predicts changes in the kinetic fractionation factor itself. For most electron transfer reactions, Marcus theory predicts that the rate constant (k) should increase log-linearly as $\Delta G_r°$ decreases, such that a reaction that is more thermodynamically favourable in the standard state is faster. Kavner and colleagues have shown that Marcus theory also describes kinetic isotope fractionation during redox reactions (Kavner *et al.*, 2005, 2008). Specifically, Marcus theory predicts that the kinetic fractionation factor (ε_{kin}) follows a linear free energy relationship for redox reactions with similar reaction mechanisms and equilibrium fractionation factors. A reaction with a lower $\Delta G_r°$ has a lower activation energy, and the difference between the activation energies of different isotopologues is also smaller. Thus, a redox reaction that is more thermodynamically favourable in the standard state is not only faster but also exhibits less kinetic fractionation.

For isotope fractionation in natural systems, the combination of electron donor and acceptor determines $\Delta G_r°$. For example, as an oxidant such as Cr(VI) enters an aquifer and travels along a flow path characterised by decreasing O_2 and E_h, Cr(VI) also encounters a changing series of abiotic reductants, *e.g.*, from trace Fe(II) sorbed onto goethite to aqueous

1. Department of Geological Sciences, Stanford University, 450 Serra Mall, Building 320, Stanford, CA 94305, USA
2. Department of Earth System Science, Stanford University, 473 Via Ortega, Stanford, CA 94305, USA
3. Energy Geosciences Division, Lawrence Berkeley National Laboratory, 1 Cyclotron Road, Berkeley, CA 94720, USA
* Corresponding author (email: joewongc@stanford.edu)

Fe(II) to Fe(II) sulphides, in broad accordance with the redox ladder (Champ *et al.*, 1979). This sequence of reductants results in a shifting $\Delta G_r°$ for the reduction of Cr(VI). If $\Delta G_r°$ also influences k and ε_{kin}, we would expect kinetic isotope fractionation during Cr(VI) reduction to change along the flow path in a predictable fashion, consistent with electrochemical experiments. To date, the expected linear relationship between ε_{kin} and $\Delta G_r°$ has not been demonstrated in natural systems.

To test for a thermodynamic control on kinetic fractionation, we examined a model system, Cr(VI) reduction by aqueous Fe(II). Chromium(VI) reduction was chosen because it consistently results in kinetic isotope fractionation (Wang *et al.*, 2015) and is actively cycled in aquifers and marine sediments, even though the multi-electron reduction is more difficult to model explicitly. Chromium naturally occurs as Cr(VI), which is generally soluble and toxic, and as Cr(III), which is both far less soluble and environmentally benign (Ball and Nordstrom, 1998). Fractionation during Cr(VI) reduction induces kinetic fractionation that enriches the remaining Cr(VI) in the heavier isotopes (Ellis *et al.*, 2002). This fractionation may be documented as positive isotopic excursions in the rock record (Ellis *et al.*, 2002; Frei *et al.*, 2009). In modern environments, Cr(VI) isotope signatures may fingerprint reduction of Cr(VI) pollution (Berna *et al.*, 2010).

The unexplained variability in ε_{kin} for Cr(VI) reduction, which ranges from -0.2 ‰ to -5 ‰, poses a barrier to interpretation of Cr isotope signatures (Qin and Wang, 2017). Although faster reduction often causes less fractionation of Cr(VI) (Sikora *et al.*, 2008; Basu and Johnson, 2012; Jamieson-Hanes *et al.*, 2014), the origin of this effect has not been established. In accordance with predictions from electrochemical experiments, we demonstrate a log-linear relationship between ε_{kin} and k for Cr(VI) reduction by aqueous Fe(II) that arises from the dependence of both ε_{kin} and k on $\Delta G_r°$. Aqueous Fe(II) is one of the fastest naturally occurring reductants of Cr(VI) at circumneutral pH (Fendorf *et al.*, 2000), but hydrolysis and organic ligation of Fe(II) alter its standard reduction potential ($E°$) such that the rate constant of Cr(VI) reduction varies by orders of magnitude, depending on the speciation of Fe(II) (Buerge and Hug, 1997, 1998). It has not been established whether changes in ε_{kin} are associated with these changes in k because fractionation during Cr(VI) reduction by aqueous Fe(II) has only been explored in a narrow pH range (Kitchen *et al.*, 2012). By changing the ligation of Fe(II), we show experimentally and theoretically that the variation in the Cr kinetic fractionation factor can be explained in terms of a linear free energy relationship.

Results

Isotope fractionation of Cr(VI) was measured during the stepwise batch reduction of Cr(VI) by Fe(II)-citrate, Fe(II)-nitrilotriacetate, and Fe(II)-salicylate at pH 5.5 and by aqueous Fe(II) at pH values ranging from 5.0 to 7.3, following the method of Kitchen *et al.* (2012). Experimental details are available in the Supplementary Information (Methods section and Table S-1). The remaining Cr(VI) was progressively enriched in heavier isotopes for all experiments. Both organic ligation of Fe(II) (Table S-2) and pH (Table S-3) affect the extent of fractionation. The observed Cr isotope fractionation can be described using a Rayleigh distillation model with a single fractionation factor ($\varepsilon = \alpha - 1$, expressed in per mille) for each experiment (Figs. 1, S-1). Every experiment was carried out in duplicate, and no duplicates show major differences from each other.

Measured fractionation factors range from -1.7 to –3.5 ‰. The 2 ‰ range nearly spans the range of all reported fractionation factors for naturally occurring abiotic reductants of Cr(VI) (Jamieson-Hanes *et al.*, 2014). All fractionation factors are smaller than equilibrium fractionation between inorganic Cr(VI) and Cr(III) species (-6 to -7 ‰), which is unlikely to have been approached within the experimental timescale (Schauble *et al.*, 2004; Wang *et al.*, 2015), as discussed further in the Supplementary Information. All fractionation is therefore assumed to be kinetic.

Fractionation factors for Cr(VI) reduction are strongly correlated with $E°$ of the Fe(II)-Fe(III) half -reaction, which is a proxy for $\Delta G_r°$ of the electron transfers between Fe(II) and Cr(VI) (Fig. 2a). For Cr(VI) reduction by an Fe(II) species with a low $E°$, for which the oxidation of Fe(II) and concomitant reduction of Cr(VI) are thermodynamically favourable, the magnitude of ε is small. Furthermore, ε is also linearly correlated with $\log(k)$, whereby a faster reaction induces less fractionation (Fig. 2b). This correlation, which is consistent with previous qualitative observations (Sikora *et al.*, 2008; Basu and Johnson, 2012; Jamieson-Hanes *et al.*, 2014), is unlikely to be caused by transport limitations in the vigorously stirred reactors (see Supplementary Information). Instead, the correlation between ε and $\log(k)$ is likely a by-product of the dependence of both variables on $E°$ of the Fe(II)-Fe(III) half-reaction (Buerge and Hug, 1997, 1998). The correlations between ε, $\log(k)$, and $E°$ are consistent with Marcus theory and previous electrochemical observations (Kavner *et al.*, 2005, 2008).

Environmental Applications

The systematic influence of $\Delta G_r°$ on ε may be used to relate isotopic effects to environmental conditions such as the abundance of organic matter and pH. For example, organic ligation of aqueous Fe(II) is significant in marine systems and many subsurface environments (Jansen *et al.*, 2003; Morel and Price, 2003). Our results show that organic ligation of Fe(II) strongly affects isotope fractionation during reduction of Cr(VI) and potentially other redox partners. Similarly, fractionation during Cr(VI) reduction by aqueous inorganic Fe(II) depends on pH. Expanding the pH range of a previous study, we find that the effective fractionation factor (ε_{eff}) for Cr(VI) reduction by Fe(II) decreases in magnitude from –4.2 ‰ at pH 4.0 (Kitchen *et al.*, 2012) to -2.2 ‰ at pH 7.3 (Figs. 1, S-1; Table S-3).

The pH dependence of ε_{eff} is caused by the shift in the effective reductant of Cr(VI) with pH. Three Fe(II) species reduce Cr(VI) under the reaction conditions: $Fe(H_2O)_6^{2+}$, $FeOH^+$, and $Fe(OH)_2^0$. Although the vast majority of Fe(II) is present as $Fe(H_2O)_6^{2+}$ for all tested pH values, the concentrations of the two hydrolysed species increase as pH increases. Because hydrolysis lowers $E°$ of the Fe(II)-Fe(III) half-reaction, making Fe(II) more susceptible to oxidation, $FeOH^+$ and $Fe(OH)_2^0$ are more thermodynamically favourable and hence faster reductants of Cr(VI) (Buerge and Hug, 1997; Pettine *et al.*, 1998). Thus, as pH increases, $FeOH^+$ and $Fe(OH)_2^0$ become the dominant reductants of Cr(VI) in turn (Fig. 3a). The fraction of Cr(VI) reduced by each species in the environmentally relevant pH range of 4-7 was quantified using two species-specific rate laws from Pettine *et al.* (1998) and Buerge and Hug (1997). Although the overall rates predicted by these models are broadly consistent, the contribution of each Fe(II) species differs.

We modelled the pH dependence of ε_{eff} using the linear free energy relationship described above by conceptualising ε_{eff} as the average of the fractionation factors for Cr(VI) reduction

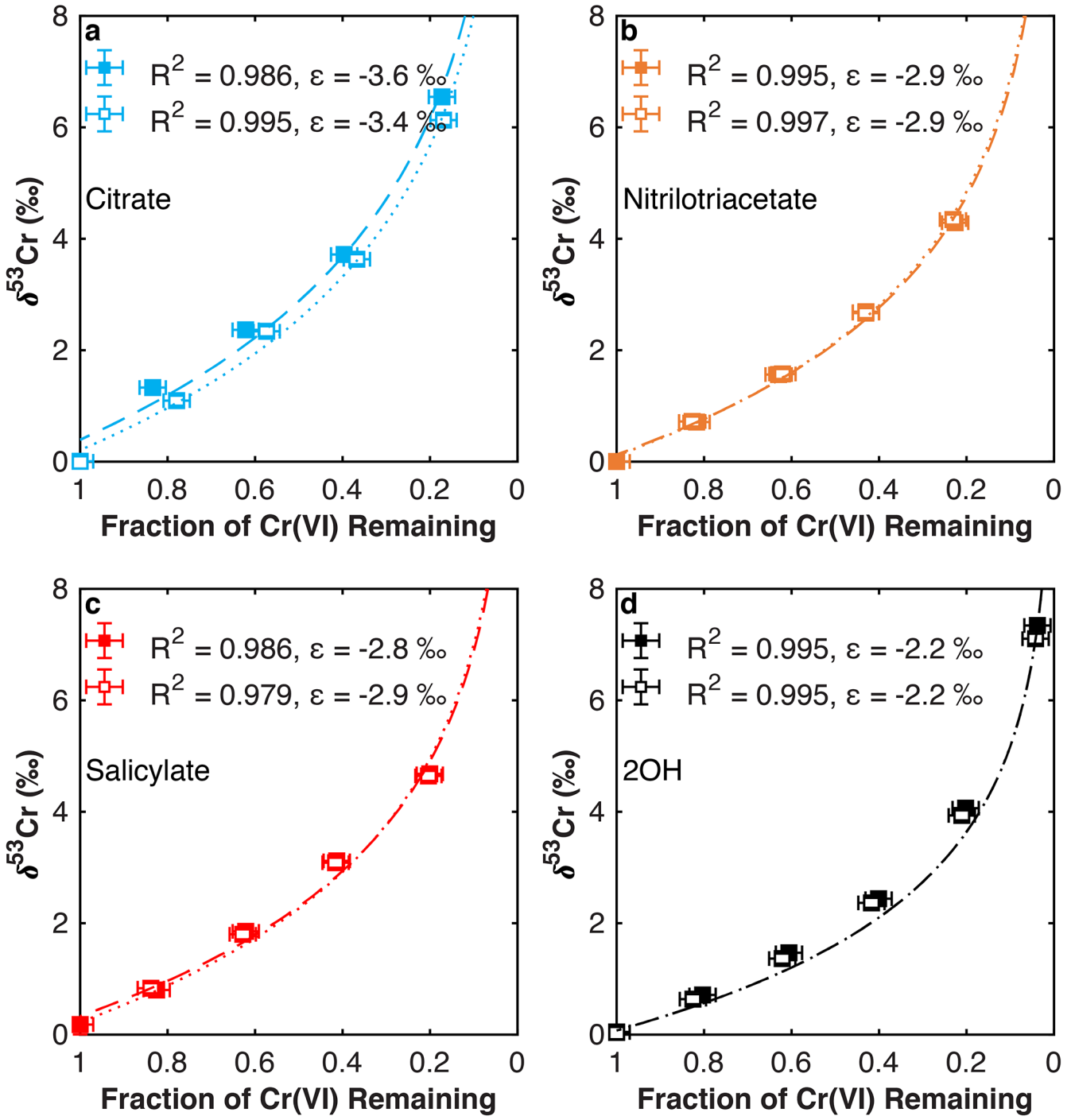

Figure 1 Isotope fractionation during Cr(VI) reduction by various aqueous Fe(II) species. Filled and open symbols in each plot show duplicate reactors. Rayleigh curves based on linear best fits are plotted as dashed lines (filled symbols) and dotted lines (open symbols). Vertical error bars (2 s.d.) are smaller than the symbols.

by each Fe(II) species (*i.e.* $Fe(H_2O)_6^{2+}$, $FeOH^+$, and $Fe(OH)_2^0$), weighted by the fraction of Cr(VI) reduced by each species. The linear free energy relationship allows the fractionation factor for $FeOH^+$ to be interpolated (ε_{OH} = -3.2 ‰), and interpolated fractionation factors for $Fe(H_2O)_6^{2+}$ and $Fe(OH)_2^0$) are indistinguishable from the measured values. Because the two rate laws predict different contributions of each Fe(II) species to the overall reduction of Cr(VI) within the studied pH range, the models also predict different trends in ε_{eff} (Fig. 3b). Although neither model fits the data exactly, the model based on the rate law of Pettine *et al.* (1998) reproduces the general shape and trend of the data far better. Discrepancies are likely due to the uncertainties for the species-specific rate constants (Fig. S-2). Isotope fractionation thus offers a second axis on which to evaluate otherwise indistinguishable rate laws and improve modelling of aqueous reduction kinetics.

Our results demonstrate a systematic relationship between ε_{kin}, k, and $\Delta G_r°$ as predicted by Marcus theory. This relationship may give rise to variable kinetic isotope effects along natural redox gradients. As conditions become more reducing and different reductants become available, $\Delta G_r°$ of Cr(VI) reduction decreases, resulting in a corresponding decrease in the magnitude of kinetic fractionation (Fig. 4). We observed this quantitatively for Cr(VI) reduction by aqueous Fe(II) species (Fig. 2) and show here that the values for a more diverse set of representative reductants are broadly consistent with the predicted trend (Ellis *et al.*, 2002;

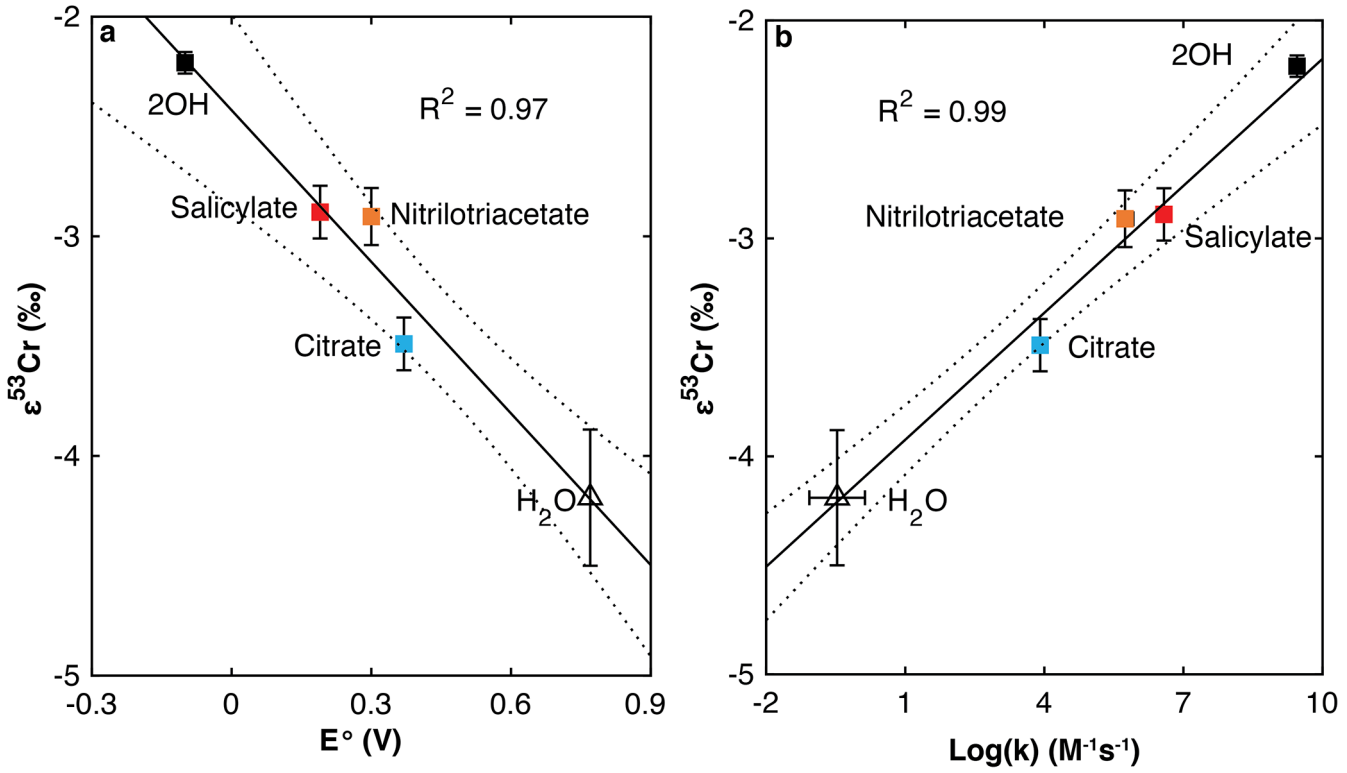

Figure 2 Linear relationships of kinetic isotope fractionation factor for Cr(VI) reduction with **(a)** the Fe(II)-Fe(III) standard reduction potential and **(b)** rate constants. Solid line shows weighted linear regression, and dotted lines show 95 % confidence interval. Each symbol shows the average fractionation factor calculated for replicate experiments. Error bars are 2 s.d. The fractionation factor for Cr(VI) reduction by $Fe(H_2O)_6^{2+}$ is taken from Kitchen *et al.* (2012), and the rate constants are taken from Buerge and Hug (1997, 1998).

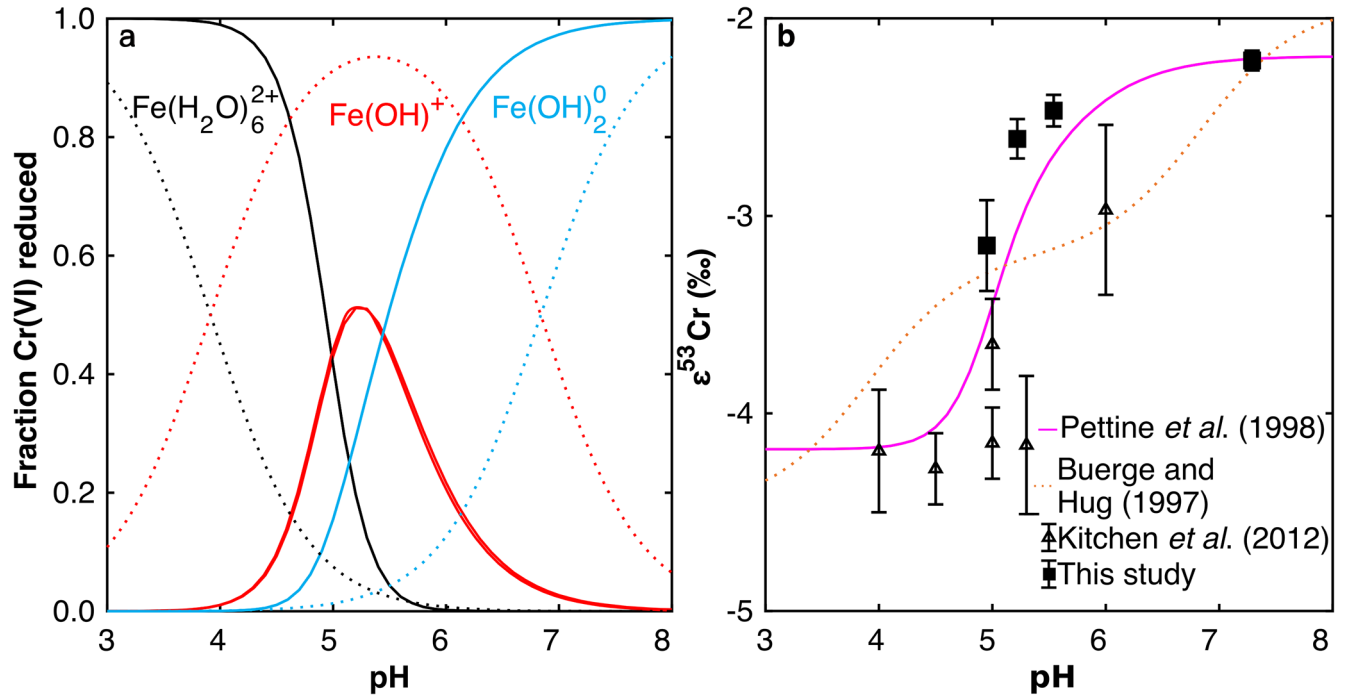

Figure 3 Effects of pH on the kinetics and isotope fractionation of Cr(VI) reduction by aqueous Fe(II). In both parts, solid lines show the model based on the rate law of Pettine *et al.* (1998); dashed lines show the model based on the rate law of Buerge and Hug (1997). **(a)** The fraction of Cr(VI) reduced by each Fe(II) species is contingent on pH-dependent Fe(II) speciation and the rate law of Cr(VI) reduction. **(b)** The effective fractionation factor is the weighted average of the fractionation factors for Cr(VI) reduction by each Fe(II) species. Error bars on the symbols in (**b**) are 2 s.d.

Basu and Johnson, 2012; Kitchen *et al.*, 2012). Thermodynamically driven kinetic isotope effects thus explain part of the scatter in observed fractionation factors. Ultimately, predictable changes in Cr kinetic fractionation along redox gradients may help to distinguish between anoxic and euxinic palaeoredox conditions and allow first order estimates of Cr(VI) fractionation in natural settings.

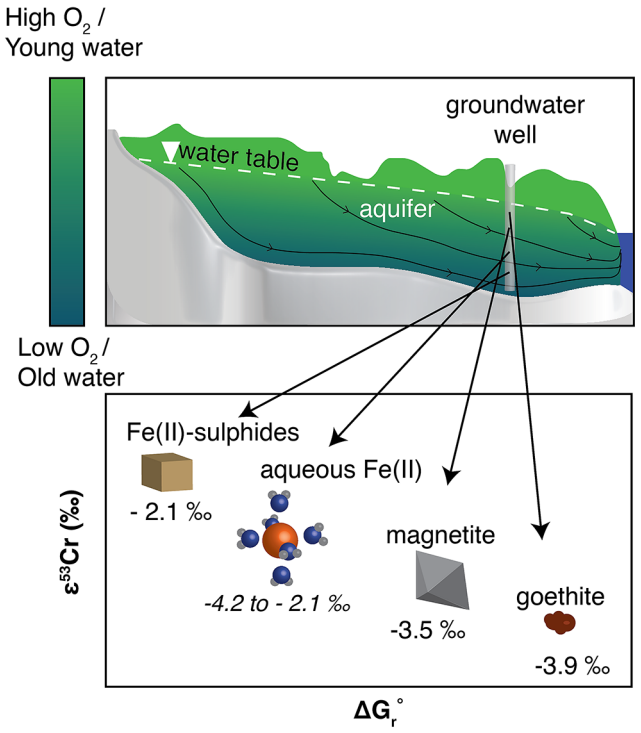

Figure 4 Schematic of Cr(VI) reduction and variations in ε_{kin} with depth, groundwater age, and oxygen levels. The dominant reductants are ordered according to their relative locations on the redox tower. Kinetic fractionation factors are taken from this study; aqueous Fe(II); Kitchen *et al.* (2012), aqueous Fe(II); Basu and Johnson (2012), Fe(II)-doped goethite and Fe(II) sulphide, and Ellis *et al.* (2002), magnetite.

Conclusions

Fundamental understanding of redox-driven kinetic fractionation will strengthen our ability to interpret environmental change, especially along redox gradients. Capturing redox-dependent kinetic isotope effects may be aided by using linear free energy relationships to interpolate fractionation factors from limited experimental data. More research is needed to evaluate the applicability of Marcus theory to other stable isotope systems, particularly during oxidation and for more complex, heterogeneous and microbially mediated redox reactions. Fractionation during Cr(VI) reduction is generally solely kinetic (Qin and Wang, 2017), so the predicted linear free energy relationship observed herein is unambiguous. In other redox-driven systems that approach isotopic equilibrium, the relationship between observed fractionation and ΔG_r° is likely more complicated. Predicting observed fractionation in these cases may require combining Marcus theory with a model that predicts the shift between kinetic and equilibrium fractionation such as that in DePaolo (2011). Combining Marcus theory with other models would also be necessary if a significant component of fractionation is not redox-driven. Nevertheless, similar trends should exist for other redox-sensitive elements; metals such as U exhibit significant fractionation upon reduction (Brown *et al.*, 2018), and traditional light stable isotope systems also may be described by linear free energy relationships (Gorski *et al.*, 2010). By permitting more precise interpretations of redox-driven isotope fractionation, the framework presented here is poised to improve our understanding of redox dynamics.

Acknowledgements

This work was supported by a National Science Foundation Career Award (EAR-1254156) to KM. CJ.-W was funded by the United States Department of Defense through a National Defense Science & Engineering Graduate Fellowship and by a Stanford Graduate Fellowship. STB. was funded by the U.S. Department of Energy, Office of Basic Energy Sciences (DE-AC02-05CH11231).

Editor: Liane G. Benning

Additional Information

Supplementary Information accompanies this letter at http://www.geochemicalperspectivesletters.org/article1909.

Cite this letter as: Joe-Wong, C., Weaver, K.L., Brown, S.T., Maher, K. (2019) Thermodynamic controls on redox-driven kinetic stable isotope fractionation. *Geochem. Persp. Let.* 10, 20–25.

References

Ball, J.W., Nordstrom, D.K. (1998) Critical Evaluation and Selection of Standard State Thermodynamic Properties for Chromium Metal and Its Aqueous Ions, Hydrolysis Species, Oxides, and Hydroxides. *Journal of Chemical & Engineering Data* 43, 895–918.

Basu, A., Johnson, T.M. (2012) Determination of Hexavalent Chromium Reduction Using Cr Stable Isotopes: Isotopic Fractionation Factors for Permeable Reactive Barrier Materials. *Environmental Science & Technology* 46, 5353–5360.

Berna, E.C., Johnson, T.M., Makdisi, R.S., Basu, A. (2010) Cr Stable Isotopes As Indicators of Cr(VI) Reduction in Groundwater: A Detailed Time-Series Study of a Point-Source Plume. *Environmental Science & Technology* 44, 1043–1048.

Brown, S.T., Basu, A., Ding, X., Christensen, J.N., DePaolo, D.J. (2018) Uranium isotope fractionation by abiotic reductive precipitation. *Proceedings of the National Academy of Sciences* 201805234.

Buerge, I.J., Hug, S.J. (1997) Kinetics and pH Dependence of Chromium(VI) Reduction by Iron(II). *Environmental Science & Technology* 31, 1426–1432.

Buerge, I.J., Hug, S.J. (1998) Influence of Organic Ligands on Chromium(VI) Reduction by Iron(II). *Environmental Science & Technology* 32, 2092–2099.

Champ, D.R., Gulens, J., Jackson, R.E. (1979) Oxidation–reduction sequences in ground water flow systems. *Canadian Journal of Earth Sciences* 16, 12–23.

DePaolo, D.J. (2011) Surface kinetic model for isotopic and trace element fractionation during precipitation of calcite from aqueous solutions. *Geochimica et Cosmochimica Acta* 75, 1039–1056.

Ellis, A.S., Johnson, T.M., Bullen, T.D. (2002) Chromium Isotopes and the Fate of Hexavalent Chromium in the Environment. *Science* 295, 2060–2062.

Fantle, M.S., DePaolo, D.J. (2007) Ca isotopes in carbonate sediment and pore fluid from ODP Site 807A: The Ca2+(aq)–calcite equilibrium fractionation factor and calcite recrystallization rates in Pleistocene sediments. *Geochimica et Cosmochimica Acta* 71, 2524–2546.

Fendorf, S., Wielinga, B.W., Hansel, C.M. (2000) Chromium Transformations in Natural Environments: The Role of Biological and Abiological Processes in Chromium(VI) Reduction. *International Geology Review* 42, 691–701.

Frei, R., Gaucher, C., Poulton, S.W., Canfield, D.E. (2009) Fluctuations in Precambrian atmospheric oxygenation recorded by chromium isotopes. *Nature* 461, 250–253.

Gorski, C.A., Nurmi, J.T., Tratnyek, P.G., Hofstetter, T.B., Scherer, M.M. (2010) Redox Behavior of Magnetite: Implications for Contaminant Reduction. *Environmental Science & Technology* 44, 55–60.

Hofmann, A.E., Bourg, I.C., DePaolo, D.J. (2012) Ion desolvation as a mechanism for kinetic isotope fractionation in aqueous systems. *Proceedings of the National Academy of Sciences* 109, 18689–18694.

Jamieson-Hanes, J.H., Lentz, A.M., Amos, R.T., Ptacek, C.J., Blowes, D.W. (2014) Examination of Cr(VI) treatment by zero-valent iron using in situ, real-time X-ray absorption spectroscopy and Cr isotope measurements. *Geochimica et Cosmochimica Acta* 142, 299–313.

Jansen, B., Nierop, K.G.J., Verstraten, J.M. (2003) Mobility of Fe(II), Fe(III) and Al in acidic forest soils mediated by dissolved organic matter: influence of solution pH and metal/organic carbon ratios. *Geoderma* 113, 323–340.

Kavner, A., Bonet, F., Shahar, A., Simon, J., Young, E. (2005) The isotopic effects of electron transfer: An explanation for Fe isotope fractionation in nature. *Geochimica et Cosmochimica Acta* 69, 2971–2979.

Kavner, A., John, S.G., Sass, S., Boyle, E.A. (2008) Redox-driven stable isotope fractionation in transition metals: Application to Zn electroplating. *Geochimica et Cosmochimica Acta* 72, 1731–1741.

Kitchen, J.W., Johnson, T.M., Bullen, T.D., Zhu, J., Raddatz, A. (2012) Chromium isotope fractionation factors for reduction of Cr(VI) by aqueous Fe(II) and organic molecules. *Geochimica et Cosmochimica Acta* 89, 190–201.

Marcus, R.A. (1964) Chemical and electrochemical electron-transfer theory. *Annual Review of Physical Chemistry* 15, 155–196.

Marcus, R.A. (1965) On the Theory of Electron-Transfer Reactions. VI. Unified Treatment for Homogeneous and Electrode Reactions. *The Journal of Chemical Physics* 43, 679–701.

Marcus, R.A. (1993) Electron transfer reactions in chemistry. Theory and experiment. *Reviews of Modern Physics* 65, 599–610.

Morel, F.M.M., Price, N.M. (2003) The Biogeochemical Cycles of Trace Metals in the Oceans. *Science* 300, 944–947.

Nielsen, L.C., DePaolo, D.J., De Yoreo, J.J. (2012) Self-consistent ion-by-ion growth model for kinetic isotopic fractionation during calcite precipitation. *Geochimica et Cosmochimica Acta* 86, 166–181.

Pettine, M., D'Ottone, L., Campanella, L., Millero, F.J., Passino, R. (1998) The reduction of chromium (VI) by iron (II) in aqueous solutions. *Geochimica et Cosmochimica Acta* 62, 1509–1519.

Qin, L., Wang, X. (2017) Chromium Isotope Geochemistry. *Reviews in Mineralogy and Geochemistry* 82, 379–414.

Schauble, E., Rossman, G.R., Taylor Jr., H.P. (2004) Theoretical estimates of equilibrium chromium-isotope fractionations. *Chemical Geology* 205, 99–114.

Sikora, E.R., Johnson, T.M., Bullen, T.D. (2008) Microbial mass-dependent fractionation of chromium isotopes. *Geochimica et Cosmochimica Acta* 72, 3631–3641.

Wang, X., Johnson, T.M., Ellis, A.S. (2015) Equilibrium isotopic fractionation and isotopic exchange kinetics between Cr(III) and Cr(VI). *Geochimica et Cosmochimica Acta* 153, 72–90.

Geochemical Perspectives Letters

Thermodynamic controls on redox-driven kinetic stable isotope fractionation

C. Joe-Wong, K.L. Weaver, S.T. Brown, K. Maher

Supplementary Information

The Supplementary Information includes:

- Methods
- Kinetic Fractionation
- Tables S-1 to S-4
- Figures S-1 and S-2
- Supplementary Information References

Methods

Reduction Experiments

All experiments were performed in an anaerobic glovebox in acid-washed amber HDPE bottles. Solutions were made with doubly deionised water sparged with N_2. Each reactor contained 20 μM Cr(VI), prepared from a 2 mM Na_2CrO_4 stock, and was buffered by 500 μM sodium acetate (pH 4-5.5) or 4-(2-hydroxyethyl)-1-piperazineethanesulfonate (HEPES) (pH 7.3). All experiments with Fe(II)-organic species were conducted at pH 5.5. Fe(II) stocks were prepared from $FeCl_2{\cdot}6H_2O$ and contained 125 μM Fe(II), 125 μM of the appropriate organic ligand, if any, and 600 μM of the appropriate buffer. A 500 μM Fe(II) stock at pH 7.3 was also prepared.

To ensure that all Cr(VI) was reduced by the intended Fe(II) species, Cr(VI) and Fe(II) were speciated at equilibrium under the reaction conditions using Visual MINTEQ 3.1 (Gustafsson, 2013). Binding constants for the organic ligands were taken from Buerge and Hug (1998). The rate of Cr(VI) reduction by each Fe(II) species present was determined from the speciation of Fe(II) and species-specific rate constants for Cr(VI) reduction by organically ligated Fe(II) (Buerge and Hug, 1998) and inorganic Fe(II) (Pettine *et al.*, 1998). As shown in Table S-1, over 99 % of Cr(VI) is reduced by the intended species under the reaction conditions for each reactor.

Following the method of Kitchen *et al.* (2012), all reactors were constantly stirred. Aliquots of Fe(II) were added to the reservoir of Cr(VI) such that 10–20 % of Cr(VI) reacted, and the reaction was allowed to continue until all the added Fe(II) reacted. An aliquot was then filtered (0.2 μm polyethersulfone), and the concentration of Cr(VI) was measured spectrophotometrically using diphenylcarbazide within 3 % reliability (Environmental Protection Agency, 1992). The fraction of Cr(VI) reduced was calculated from the initial concentration of Cr(VI), the measured concentration of Cr(VI), the mass of the reactor before the addition of Fe(II), the mass of the reactor after the addition of Fe(II), and the mass of the reactor after sampling in order to account for changing solution volumes (Kitchen *et al.*, 2012).

Chromium(VI) Separation

To correct for fractionation due to sample preparation, Cr purification, and instrumental mass bias, a double isotope spike solution (^{50}Cr and ^{54}Cr) was prepared. Purified ^{50}Cr and ^{54}Cr metal was obtained from Isoflex (San Francisco, CA) and gravimetrically prepared into a solution with a target ^{50}Cr/^{54}Cr of approximately 1 (Rudge *et al.*, 2009). For calibration, the spike was combined with the NIST SRM 979 Cr standard at various spike-sample ratios and the resulting isotopic compositions were measured. Using the accepted values for NIST SRM 979, the exact isotopic composition of the spike was determined. These spike values were used as "knowns" in a system of equations to simultaneously determine an instrumental mass bias factor, the fraction of spike in the spike-sample mixture, and the Cr isotopic composition of the sample. A new batch of the spike was oxidised to Cr(VI) using hydrogen peroxide and ammonium hydroxide for each run, and the oxidised spike added to each sample such that spike Cr:total Cr(VI) = 0.4. The spike was allowed to equilibrate overnight with the sample. Samples from the inorganic Fe(II) reactors were then purified using anion exchange columns (AG1X8 resin, 100-200 mesh, Eichrom) (Ellis *et al.*, 2002; Basu and Johnson, 2012). The anion-exchange resin was pre-cleaned with 2N HNO_3 and flushed with doubly deionised water until the effluent reached circumneutral pH. In brief, cations were eluted with 0.1 N HCl. Sorbed Cr(VI) was then reduced to Cr(III) and eluted with hydrogen peroxide and 2 N HNO_3. Any remaining Fe was removed by taking samples up in 6 N HCl and putting them through a second anion exchange column (AG1X8 resin, 100–200 mesh, Eichrom). Negatively charged $FeCl_4^-$ was retained on the anion resin, and Cr(III) was eluted with 6 N HCl. Organic residue from the resin was destroyed by repeatedly treating the samples with 30 wt. % hydrogen peroxide and 15 N HNO_3. Column yields were approximately 70 %.

Samples from Fe(II)-organic reactors required further treatment because the organic ligands form soluble complexes with Cr(III) and Fe(III) and have a high affinity for AG1X8 anion resin, thwarting easy separation of Cr(VI) from Cr(III). After spike equilibration, samples were shaken overnight with pre-cleaned (2 N HNO_3) cation resin (AG50WX8, 200-400 mesh, Bio-Rad). The cation resin was then filtered out, and the samples were purified with anion exchange columns as detailed above. The effectiveness of the separation of Cr(VI) from Cr(III) was evaluated using mass balance equations. For the original, unprocessed sample, the overall isotopic composition of Cr(VI) and Cr(III) must be the same as the original isotopic composition of Cr(VI) prior to reaction:

$$\delta^{53}\mathrm{Cr(VI)}_0 = \frac{\mathrm{Cr(VI)_{sample}}}{\mathrm{Cr(total)_{sample}}}\delta^{53}\mathrm{Cr(VI)} + \frac{\mathrm{Cr(III)_{sample}}}{\mathrm{Cr(total)_{sample}}}\delta^{53}\mathrm{Cr(III)} \qquad \text{(Eq. S-1)}$$

In Equation S-1, the original isotopic composition of Cr(VI) prior to reaction (δ^{53}Cr(VI)$_0$) was measured for every reactor. The fraction of Cr(VI)$_{sample}$/Cr(total)$_{sample}$ was calculated as discussed above, and

$$\frac{\mathrm{Cr(III)_{sample}}}{\mathrm{Cr(total)_{sample}}} = 1 - \frac{\mathrm{Cr(VI)_{sample}}}{\mathrm{Cr(total)_{sample}}} \qquad \text{(Eq. S-2)}$$

Thus, the remaining unknowns are δ^{53}Cr(VI) and δ^{53}Cr(III).

A similar mass balance equation was constructed for the processed, measured sample, where the measured isotopic composition of Cr is the weighted average of the true isotopic composition of Cr(VI) and the isotopic composition of Cr(III), if any Cr(III) remains in the sample:

$$\delta^{53}\mathrm{Cr_{measured}} = \frac{\mathrm{Cr(VI)_{measured}}}{\mathrm{Cr(total)_{measured}}}\delta^{53}\mathrm{Cr(VI)} + \frac{\mathrm{Cr(III)_{measured}}}{\mathrm{Cr(total)_{measured}}}\delta^{53}\mathrm{Cr(III)} \qquad \text{(Eq. S-3)}$$

Here the unknowns are δ^{53}Cr(VI), δ^{53}Cr(III), and the fraction of Cr(VI)/Cr(total) in the processed sample. The last quantity was calculated by isotope dilution. The amount of Cr(VI) in the sample was determined spectrophotometrically as discussed above, and the amount of spike Cr added to sample was also known from the mass of the spike and its concentration. The amount of Cr(III) was then calculated from the proportion p of the spike in the measured sample (Rudge *et al.*, 2009):

$$\mathrm{p} = \frac{\mathrm{Cr_{spike}}}{\mathrm{Cr(VI)_{measured}} + \mathrm{Cr(III)_{measured}}} \qquad \text{(Eq. S-4)}$$

The fraction of Cr(III) in the processed, measured sample was insignificant except for the Fe(II)-citrate experiments, for which Cr(III) comprised 14 % of the processed, measured samples on average. Thus, ultimately the two mass balance equations can be used to calculate the two remaining unknowns, δ^{53}Cr(VI) and δ^{53}Cr(III).

Isotopic Analysis

Chromium isotopic ratios were measured at Lawrence Berkeley National Laboratory on a multi-collector inductively-coupled-plasma mass spectrometer (Neptune Plus, Thermo Fisher) in high resolution. Purified samples were taken up in 2 % nitric acid to yield ~2 μg ^{52}Cr/mL. Isotopic compositions are reported in δ notation as deviations from NIST SRM 979:

$$\delta^{53}\mathrm{Cr} = \left(\frac{\left({}^{53}\mathrm{Cr}/{}_{52}\mathrm{Cr}\right)_{\mathrm{sample}}}{\left({}^{53}\mathrm{Cr}/{}_{52}\mathrm{Cr}\right)_{979}} - 1 \right) \qquad \text{(Eq. S-5)}$$

All measured δ values were corrected for instrumental mass fractionation by deconvoluting the double spike (Rudge *et al.*, 2009). Spiked standard NIST SRM 979 (δ^{53}Cr defined as 0 ‰) was measured between every three samples to assess instrument mass bias drift. The long-term average δ^{53}Cr of the standard was 0.01 ± 0.09 ‰ (2S.D.). Oxidised NIST SRM 979 processed in parallel with samples had an identical δ^{53}Cr of 0.01 ‰. To further estimate the uncertainty associate with these measurements, 13 samples were measured in duplicate, with an almost identical uncertainty of 0.1 ‰ based on twice the root-mean-squared difference.

Fractionation factors were determined using the linearised Rayleigh equation. The linear regression was weighted using uncertainties in both the fraction of Cr(VI) reduced and the measured isotope ratio, and uncertainties for the fractionation factors are two standard deviations of the slope of this regression (York *et al.*, 2004). Weighted and unweighted linear regressions yield identical fractionation factors within uncertainty for all experiments.

As discussed in the main text, the effective fractionation factor ε_{eff} for Cr(VI) reduction by aqueous inorganic Fe(II) is the average of the species-specific fractionation factors for all the relevant Fe(II) species ($Fe(H_2O)_6^{2+}$, $FeOH^+$, and $Fe(OH)_2^0$), weighted by the fraction of Cr(VI) that is reduced by each Fe(II) species. The species-specific fractionation factors can be quantitatively estimated from $E°$ of each species using the linear free energy relationship shown in Figure 1. The fraction of Cr(VI) reduced by each Fe(II) species depends on the amount of each Fe(II) species present and on the species-specific rate constant for Cr(VI) reduction. To determine the amount of each Fe(II) species present, Cr(VI) and Fe(II) were speciated at equilibrium under the reaction conditions using Visual MINTEQ 3.1 (Gustafsson, 2013). Species-specific rate constants for Cr(VI) reduction by Fe(II) were taken from Pettine *et al*. (1998) and Buerge and Hug (1997), and ε_{eff} was calculated as below:

$$\varepsilon_{eff} = \frac{k_{H_2O}\times[Fe(H_2O)_6{}^{2+}]\times\varepsilon_{H_2O} + k_{OH}\times[Fe(OH)^+]\times\varepsilon_{OH} + k_{2OH}\times[Fe(OH)_2{}^0]\times\varepsilon_{2OH}}{k_{H_2O}\times[Fe(H_2O)_6{}^{2+}] + k_{OH}\times[Fe(OH)^+] + k_{2OH}\times[Fe(OH)_2{}^0]} \qquad \text{(Eq. S-6)}$$

where k_{H2O} and ε_{H2O} refer to the rate constant and fractionation factor for $Fe(H_2O)_6^{2+}$, et cetera. As shown in Figure S-2, the reported uncertainties in the rate constants from Pettine *et al.* (1998) propagate to relatively large uncertainties in the modelled ε_{eff}. Uncertainties were not propagated for the rate constants of Buerge and Hug (1997) because they are so large (*e.g.*, k_{H2O} = 0.34 ± 0.47 $M^{-1}s^{-1}$) that they make the model meaningless.

Kinetic Fractionation

Chromium fractionation during Cr(VI) reduction is typically expected to be kinetic because the back-reaction is minimal (Wang *et al.*, 2015; Qin and Wang, 2017). The product Cr(III) generally forms a highly insoluble precipitate that is not easily re-oxidised (Pan *et al.*, 2019), and even aqueous Cr(III) is slow to react (Wang *et al.*, 2015). However, in the experiments presented here where Cr(VI) is reduced by organically ligated Fe(II), the product Cr(III) may complex with the organic ligand (Buerge and Hug, 1998). It is possible that organically ligated Cr(III) may reach isotopic equilibrium with anionic Cr(VI) faster than aqueous inorganic Cr(III) ($Cr(H_2O)_6^{3+}$) or a Cr(III) precipitate. Nevertheless, it is unlikely that the observed fractionation of Cr is equilibrium or even a mixture of kinetic and equilibrium fractionation for several reasons. First, if isotopic exchange between Cr(VI) and Cr(III) is fast in these experiments, this should be reflected in the instrumental mass fractionation factor (β) determined by deconvoluting the ^{50}Cr/^{54}Cr double spike (Rudge *et al.*, 2009). Despite its name, β in fact reflects all fractionation between the addition of the spike to the sample and measurement of the isotopic ratios, which would include any equilibrium fractionation between Cr(VI) and Cr(III) in the spiked sample. The speciation of the spike was the same as the sample Cr(VI) (*i.e.* $HCrO_4^-/CrO_4^{2-}$), and the spike was allowed to equilibrate with the sample overnight. Each experiment only lasted a few days, so if the sample Cr(VI) approached isotopic equilibrium with the sample Cr(III) within the experimental timescale, the spike Cr(VI) should also approach isotopic equilibrium with the sample Cr(III) prior to separation. If significant isotopic exchange between the spike Cr(VI) and the sample Cr(III) occurs, then β for samples from the reactors with organically ligated Fe(II) should reflect this as well as fractionation from the ion exchange resins and in the

MC-ICP-MS instrument. Thus, sample β values should differ from β values for the SRM 979 standards, which only reflect fractionation from one ion exchange resin and the MC-ICP-MS instrument. No major differences between sample and standard β values were observed, so significant isotopic exchange between Cr(VI) and Cr(III) is unlikely to have occurred.

Furthermore, it is unlikely that isotopic equilibrium between Cr(VI) and Cr(III) can be approached in these experiments. Reaching isotopic equilibrium implies reaching chemical equilibrium (Beard *et al.*, 2003), but the kinetics of Cr(VI) reduction by these organically ligated Fe(II) species under the conditions of the experiment concentrations can be fit well with a unidirectional reaction (Cr(VI) → Cr(III)) and do not show any sign of back-formation of Cr(VI) (Buerge and Hug, 1998). The same lack of back-reaction has been seen for a wide variety of other Cr(VI) reduction reactions, including reduction by other aqueous Fe(II) species, hydrogen sulphide, and Fe(II/III)-bearing clay minerals (Buerge and Hug, 1997; Joe-Wong *et al.*, 2017; Pettine *et al.*, 1994). Isotopic equilibrium between aqueous inorganic Cr(VI) and Cr(III) species is approached on the order of years, with a half-life of nearly 6 years at concentrations more than 1000 times greater than in these experiments (Wang *et al.*, 2015). It is possible that in experiments with organically ligated Fe(II), Cr(III) may complex with the organic ligand (Buerge and Hug, 1998), and isotopic equilibrium between anionic Cr(VI) and organically complexed Cr(III) may be faster than equilibrium with $Cr(H_2O)_6^{3+}$. However, the rate of isotopic exchange for organically ligated Cr(III) would need to be at least six orders of magnitude faster than the rate for $Cr(H_2O)_6^{3+}$ for samples to reach isotopic equilibrium over the course of each experiment, which only lasted a few days and involved micromolar concentrations of Cr. Finally, the observed fractionation is likely too small to be equilibrium. Although there are no theoretical calculations of equilibrium fractionation factors between organically ligated and inorganic Cr(III), typically equilibrium fractionation between organically and inorganically ligated transition metals is smaller than 0.5 ‰ (Jouvin *et al.*, 2009; Morgan *et al.*, 2010; Fujii *et al.*, 2014). Thus, equilibrium fractionation between Cr(VI) and organically ligated Cr(III) would be expected to be roughly between -5.5 and -7.5 ‰ based on estimated equilibrium fractionation factors between Cr(VI) and inorganic Cr(III) (-6 to -7 ‰) (Schauble *et al.*, 2004; Wang *et al.*, 2015). The measured fractionation factors are much smaller than this and likely reflect kinetic fractionation.

The observed fractionation could also potentially be affected by physical heterogeneity in insufficiently mixed reactors, where slow diffusion of the Fe(II) stock may diminish the magnitude of measured fractionation (Kitchen *et al.*, 2012). To minimize such transport limitations, reactors were constantly stirred, and the concentration of the Fe(II) stock was low so that injecting the Fe(II) stock into the reactor would not create temporary zones with extremely high Fe(II) concentrations in which Cr(VI) reduction might be diffusion-limited. The potential for any remaining effects on measured fractionation was investigated for the fast reduction of Cr(VI) by $Fe(OH)_2^0$ at pH 7.3 (Buerge and Hug, 1997; Pettine *et al.*, 1998). To enhance heterogeneity immediately after adding the Fe(II) stock, the concentration of the added stock was increased fourfold from 125 μM to 500 μM and its volume correspondingly decreased. The measured fractionation decreased from -2.21 ± 0.05 ‰ to -1.89 ± 0.08 ‰ (Fig. S-1, Table S-4). Further increasing transport limitations by both increasing the stock concentration and decreasing the stir speed of the reactor from 900 to 300 rpm caused a slight additional decrease in ε to -1.71 ± 0.09 ‰. Although these effects are not insignificant, they are much smaller than the 2 ‰ range in kinetic fractionation observed by changing the ligation of Fe(II), which is more plausibly explained using the Marcus-theory-based model presented in the main text.

Supplementary Tables

Table S-1 Each column shows for a given reactor the predicted rate of Cr(VI) reduction and fraction of Cr(VI) reduced by each Fe(II) species present (Fe(II)-organic, $Fe(H_2O)_6^{2+}$, $Fe(OH)^+$, and $Fe(OH)_2^0$).

Reactor	*Ligand*	H_2O	Citrate	Nitrilotri-acetate	Salicylate	2OH
Rate of Cr(VI) Reduction (μM/s)	*Organic*	n/a	1.81×10^{-2}	5.45	2.02×10^{1}	n/a
	H_2O	9.36×10^{-4}	1.09×10^{-5}	2.43×10^{-7}	2.13×10^{-6}	4.85×10^{-8}
	OH	9.69×10^{-6}	3.20×10^{-6}	7.16×10^{-8}	6.28×10^{-7}	2.00×10^{-3}
	2OH	3.48×10^{-7}	9.14×10^{-8}	2.04×10^{-9}	1.79×10^{-8}	1.43×10^{-1}
Fraction of Cr(VI) Reduced	*Organic*	n/a	1.00	1.00	1.00	n/a
	H_2O	0.99	0.00	0.00	0.00	0.00
	OH	0.01	0.00	0.00	0.00	0.01
	2OH	0.00	0.00	0.00	0.00	0.99

Table S-2 Changes in isotopic composition during Cr(VI) reduction by aqueous Fe(II) species. Each pair of columns shows a duplicate reactor.

Reductant	Fraction Cr(VI) Remaining	δ^{53}Cr(VI) (‰)	Fraction Cr(VI) Remaining	δ^{53}Cr(VI) (‰)
Fe(citrate)	1	-0.02	1	0.01
	0.83	1.33	0.78	1.09
	0.62	2.37	0.57	2.34
	0.40	3.72	0.37	3.63
	0.17	6.55	0.17	6.13
Fe(nitrilotriacetate)	1	0.00	1	-0.02
	0.82	0.71	0.83	0.72
	0.63	1.56	0.62	1.57
	0.43	2.69	0.43	2.67
	0.23	4.29	0.23	4.34
Fe(salicylate)	1	0.18	1	-0.09
	0.83	0.80	0.84	0.83
	0.62	1.85	0.63	1.80
	0.41	3.12	0.42	3.09
	0.20	4.68	0.20	4.64
$Fe(OH)_2$	1	0.04	1	0.05
	0.80	0.71	0.83	0.64
	0.61	1.47	0.62	1.36
	0.40	2.44	0.42	2.36
	0.20	4.06	0.21	3.93
	0.04	7.34	0.04	7.11

Table S-3 Changes in isotopic compositions during Cr(VI) reduction by aqueous Fe(II) at different pH values. Each pair of columns shows a duplicate reactor.

pH	Fraction Cr(VI) Remaining	δ^{53}Cr(VI) (‰)	Fraction Cr(VI) Remaining	δ^{53}Cr(VI) (‰)
4.95	1	0.05	1	0.03
	0.83	0.82	0.83	0.84
	0.61	1.76	0.61	1.76
	0.40	2.98	0.40	2.97
5.22	1	0.18	1	0.01
	0.74	0.80	0.82	0.90
	0.50	1.85	0.58	2.09
	0.27	3.12	0.33	3.51
	--	--	0.11	5.62
5.54	1	0.04	1	0.05
	0.79	0.83	0.78	0.92
	0.57	1.79	0.56	1.98
	0.34	3.06	0.32	3.42

Table S-4 Changes in isotopic compositions during Cr(VI) reduction by aqueous Fe(II) at pH 7.3 under different transport conditions. Each pair of columns shows a duplicate reactor.

Reductant	Fe(II) Stock Concentration (µM)	Stir Speed (rpm)	Fraction Remaining Cr(VI)	δ^{53}Cr(VI) (‰)
$Fe(OH)_2$	500	900	1	0.08
			0.74	0.59
			0.60	1.27
			0.38	2.05
			0.19	3.44
			0.04	6.22
$Fe(OH)_2$	500	300	1	0.06
			0.83	0.55
			0.62	1.12
			0.41	1.89
			0.21	2.91
			0.05	5.40

Supplementary Figures

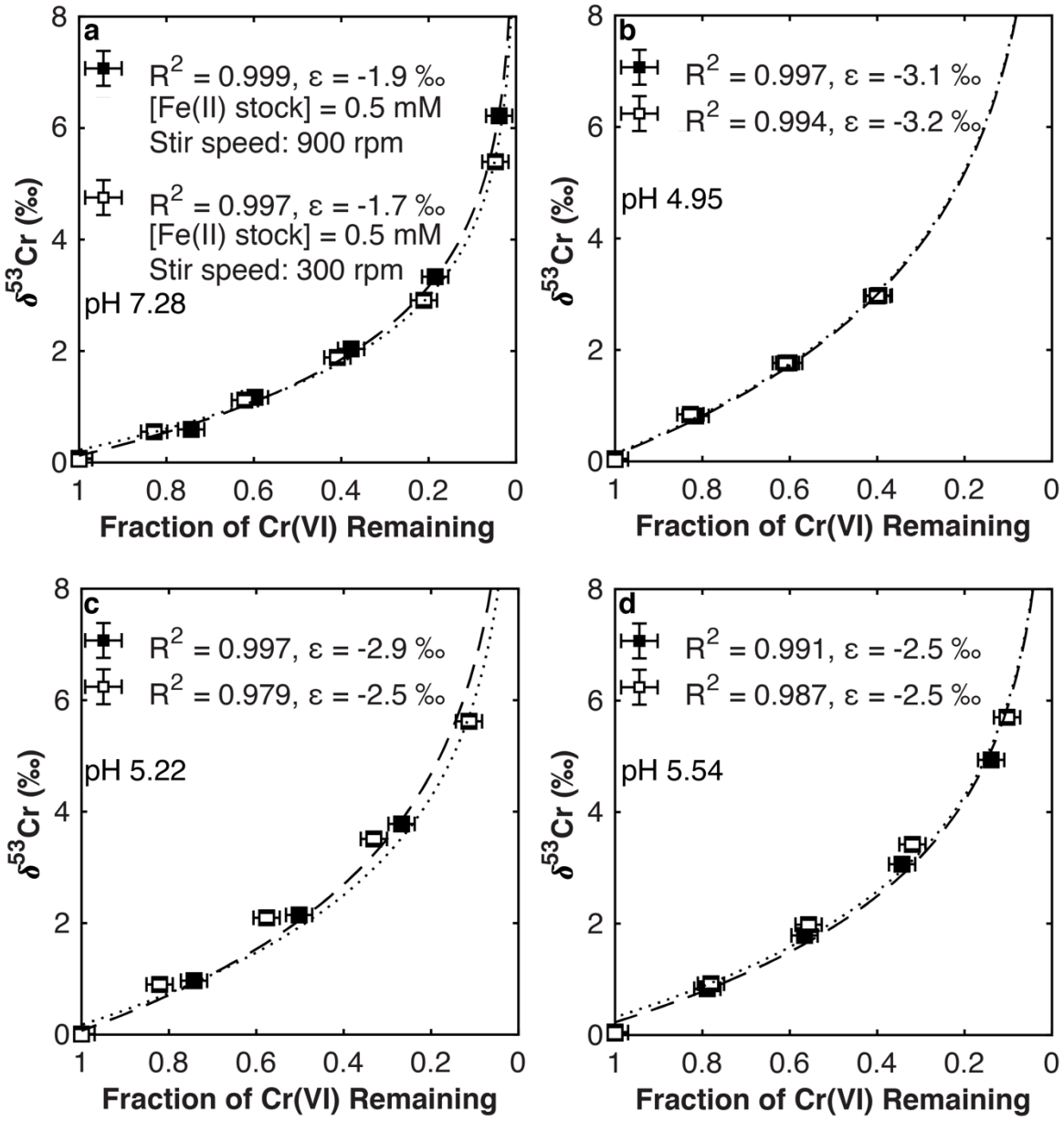

Figure S-1 Rayleigh plots of isotope fractionation during Cr(VI) reduction by aqueous Fe(II) at **(a)** different experimental conditions and **(b-d)** pH values. Filled and open symbols in each plot show duplicate reactors. Rayleigh curves based on linear best fits are plotted as dashed lines (filled symbols) and dotted lines (open symbols). Vertical error bars (2 S.D.) are smaller than the symbols.

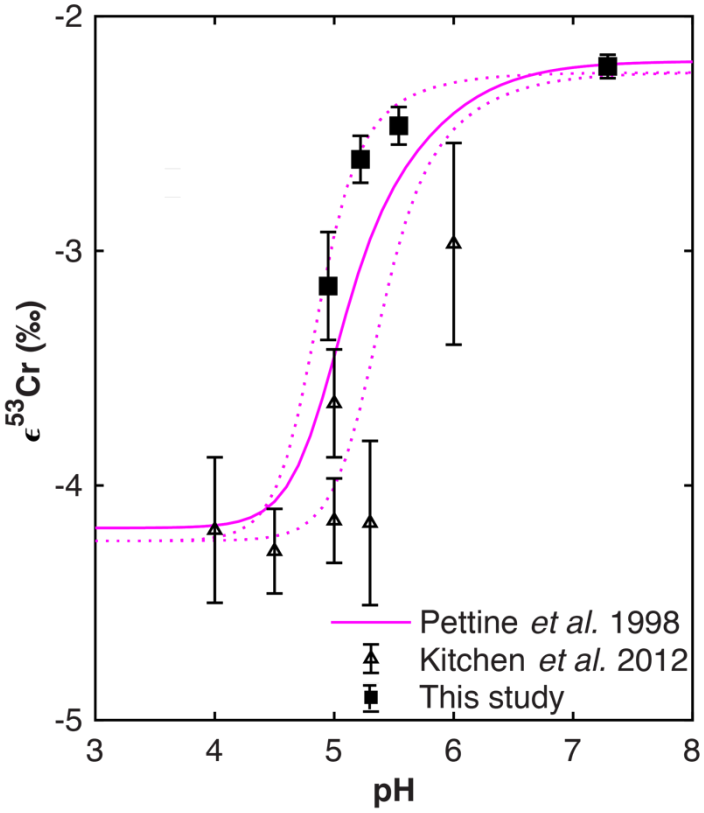

Figure S-2 Uncertainties on the modelled pH dependence of isotope fractionation of Cr(VI) reduction by aqueous Fe(II). The solid line is based on the species-specific rate constants of Pettine *et al*. (1998), and the dashed lines show variations in the model when the species-specific rate constants are varied by 2S.D. as reported by Pettine *et al.* (1998).

Supplementary Information References

Basu, A., Johnson, T.M. (2012) Determination of Hexavalent Chromium Reduction Using Cr Stable Isotopes: Isotopic Fractionation Factors for Permeable Reactive Barrier Materials. *Environmental Science & Technology* 46, 5353–5360.

Beard, B.L., Johnson, C.M., Skulan, J.L., Nealson, K.H., Cox, L., Sun, H. (2003) Application of Fe isotopes to tracing the geochemical and biological cycling of Fe. *Chemical Geology* 195, 87–117.

Buerge, I.J., Hug, S.J. (1997) Kinetics and pH Dependence of Chromium(VI) Reduction by Iron(II). *Environmental Science & Technology* 31, 1426–1432.

Buerge, I.J., Hug, S.J. (1998) Influence of Organic Ligands on Chromium(VI) Reduction by Iron(II). *Environmental Science & Technology* 32, 2092–2099.

Ellis, A.S., Johnson, T.M., Bullen, T.D. (2002) Chromium Isotopes and the Fate of Hexavalent Chromium in the Environment. *Science* 295, 2060–2062.

Environmental Protection Agency (1992) EPA Method 7196A. Environmental Protection Agency.

Fujii, T., Moynier, F., Blichert-Toft, J., Albarède, F. (2014) Density functional theory estimation of isotope fractionation of Fe, Ni, Cu, and Zn among species relevant to geochemical and biological environments. *Geochimica et Cosmochimica Acta* 140, 553–576.

Gustafsson, J.P. (2013) *Visual MINTEQ*. KTH, Stockholm, Sweden.

Joe-Wong, C., Brown, G.E., Maher, K. (2017) Kinetics and Products of Chromium(VI) Reduction by Iron(II/III)-Bearing Clay Minerals. *Environmental Science & Technology* 51, 9817–9825.

Jouvin, D., Louvat, P., Juillot, F., Maréchal, C.N., Benedetti, M.F. (2009) Zinc Isotopic Fractionation: Why Organic Matters. *Environmental Science & Technology* 43, 5747–5754.

Kitchen, J.W., Johnson, T.M., Bullen, T.D., Zhu, J., Raddatz, A. (2012) Chromium isotope fractionation factors for reduction of Cr(VI) by aqueous Fe(II) and organic molecules. *Geochimica et Cosmochimica Acta* 89, 190–201.

Morgan, J.L.L., Wasylenki, L.E., Nuester, J., Anbar, A.D. (2010) Fe Isotope Fractionation during Equilibration of Fe–Organic Complexes. *Environmental Science & Technology* 44, 6095–6101.

Pan, C., Liu, H., Catalano, J.G., Wang, Z., Qian, A., Giammar, D.E. (2019) Understanding the Roles of Dissolution and Diffusion in Cr(OH)3 Oxidation by δ-MnO2. *ACS Earth and Space Chemistry* 3, 357–365.

Pettine, M., D'Ottone, L., Campanella, L., Millero, F.J., Passino, R. (1998) The reduction of chromium (VI) by iron (II) in aqueous solutions. *Geochimica et Cosmochimica Acta* 62, 1509–1519.

Pettine, M., Millero, F.J., Passino, R. (1994) Reduction of chromium (VI) with hydrogen sulfide in NaCl media. *Marine Chemistry* 46, 335–344.

Qin, L., Wang, X. (2017) Chromium Isotope Geochemistry. *Reviews in Mineralogy and Geochemistry* 82, 379–414.

Rudge, J.F., Reynolds, B.C., Bourdon, B. (2009) The double spike toolbox. *Chemical Geology* 265, 420–431.

Schauble, E., Rossman, G.R., Taylor Jr., H.P. (2004) Theoretical estimates of equilibrium chromium-isotope fractionations. *Chemical Geology* 205, 99–114.

Wang, X., Johnson, T.M., Ellis, A.S. (2015) Equilibrium isotopic fractionation and isotopic exchange kinetics between Cr(III) and Cr(VI). *Geochimica et Cosmochimica Acta* 153, 72–90.

York, D., Evensen, N.M., Martínez, M.L., De Basabe Delgado, J. (2004) Unified equations for the slope, intercept, and standard errors of the best straight line. *American Journal of Physics* 72, 367–375.